blood

Prepublished online Mar 8, 2011;
doi:10.1182/blood-2010-11-321596

A novel calcium-binding site of von Willebrand factor A2 domain regulates its cleavage by ADAMTS13

Minyun Zhou, Xianchi Dong, Carsten Baldauf, Hua Chen, Yanfeng Zhou, Timothy A. Springer, Xinping Luo, Chen Zhong, Frauke Gräter and Jianping Ding

Blood (print ISSN 0006-4971, online ISSN 1528-0020), is published weekly by the American Society of Hematology, 2021 L St, NW, Suite 900, Washington DC 20036.

A novel calcium-binding site of von Willebrand factor A2 domain regulates its cleavage by ADAMTS13

Minyun Zhou[1,2,$], Xianchi Dong[1,2,$], Carsten Baldauf [3,#], Hua Chen[4], Yanfeng Zhou[5], Timothy A. Springer[5], Xinping Luo[4], Chen Zhong[1], Frauke Gräter[3,6], and Jianping Ding[1,*]

[1]State Key Laboratory of Molecular Biology and Research Center for Structural Biology, Institute of Biochemistry and Cell Biology, Shanghai Institutes for Biological Sciences, Chinese Academy of Sciences, and [2]Graduate School of Chinese Academy of Sciences, 320 Yue-Yang Road, Shanghai 200031, China; [3]Key Laboratory of Computational Biology of Chinese Academy of Sciences, CAS-MPG Partner Institute for Computational Biology, Shanghai Institutes for Biological Sciences, Chinese Academy of Sciences, 320 Yue-Yang Road, Shanghai 200031, China; [4]Huashan Hospital, Fudan Medical School, Shanghai 200040, China; [5]Immune Disease Institute, Children's Hospital Boston and Department of Pathology, Harvard Medical School, 3 Blackfan Circle, Boston, MA 02115, USA; [6]Heidelberg Institute for Theoretical Studies, Heidelberg, Germany.

Running title: Crystal structure of VWF A2 domain

[*]**Correspondence**: Dr. Jianping Ding, 320 Yue-Yang Road, Shanghai 200031, China, Phone: (086-21)-5492-1619, Fax: (086-21)-5492-1116, E-mail: jpding@sibs.ac.cn.

[$]These authors contributed equally.

[#]Present address: Fritz-Haber-Institut der Max-Planck-Gesellschaft, Theory Department, Faradayweg 4-6, D-14195 Berlin-Dahlem,Germany.

Category: Thrombosis and hemostasis.

Abbreviations: VWF, von Willebrand factor; VWD, von Willebrand disease; VWA domain, von Willebrand factor A domain; ssA2, a disulfide cross-linked A2 domain; wtA2, wild-type A2 domain; MD, molecular dynamics.

Key words: VWF, A2 domain, ADAMTS13, calcium, regulation, cleavage, hemostasis.

Abstract

The proteolysis of von Willebrand factor (VWF) by ADAMST13 is an essential step for regulation of its hemostatic and thrombogenic potential. The cleavage occurs at strand β4 in the structural core of the A2 domain of VWF, thus unfolding of the A2 domain is pre-requisite for the cleavage. Here we present the crystal structure of an engineered A2 domain, which exhibits significant difference in the α3-β4 loop compared with the previously reported structure of the wild-type A2. Intriguingly, a metal ion was detected at a site formed mainly by the C-terminal region of the α3-β4 loop, and later identified to be Ca^{2+} with various biophysical and biochemical studies. Force probe molecular dynamics simulations of a modeled structure of the wild-type A2 that features the discovered Ca^{2+}-binding site revealed that an increase of the force is needed to unfold strand β4 when Ca^{2+} is bound. Consistently, cleavage assays demonstrated that the Ca^{2+} binding stabilizes the A2 domain and impedes its unfolding, and consequently protects it from cleavage by ADAMTS13. Taken together, we have revealed a novel Ca^{2+}-binding site at the A2 domain of VWF and demonstrated interplay of Ca^{2+} and force in the regulation of VWF and primary hemostasis.

Introduction

von Willebrand factor (VWF) plays an important role in primary hemostasis through mediating platelet adhesion. VWF is stored in endothelial Weibel-Palade bodies and platelet α-granules as glycosylated multimers consisting of the largest multimeric species, i.e. ultra-large VWF.[1-4] Upon stimulation the VWF multimers are released into the circulating blood or subendothelial matrix. Within two hours after release into the vessel, the secreted ultra-large VWF multimers are converted to smaller multimers ranging from 500 to 20,000 kDa by ADAMTS13 proteolysis.[5-8] The cleavage site for ADAMTS13 resides at the Tyr1605-Met1606 bond in the A2 domain,[1,9] which is a cryptic site buried in the central β-strand in the intact, folded A2 domain and thus is inaccessible to ADAMTS13.[10]

More than a decade ago it was observed that shear stress promotes the process of VWF proteolysis.[11] To date, a large body of evidence has supported the notions that the conformation of VWF fibers is altered by shear stress[12] and that unfolding of VWF by shear stress led to an enhanced susceptibility of the VWF to ADAMTS13 proteolysis.[13-15] As the hemostatic potential of VWF greatly increases with its length, cleavage by ADAMTS13 provides an important regulatory mechanism for primary hemostasis. The cleavage process is precisely regulated *in vivo* and dysfunction of the regulation can lead to severe consequences. For example, mutations in VWF that cause increased susceptibility of VWF to ADAMTS13 will lead to a shift of the multimer distribution to smaller forms which have less hemostatic potential and thus result in continuing bleeding known as different types of von Willebrand disease (VWD).[16,17] In particular, most mutations in the A2 domain which are associated with VWD type 2A, the common qualitative defect of VWD, result in enhanced proteolytic succeptibility.[18]

Recently, it was clearly shown that unfolding of A2 is required for its cleavage by ADAMTS13, and an intermediate state exists with unfolding of the C-terminal region up to

and including the β4 strand where the cleavage site is located.[19] Further information of stepwise unfolding of A2 under tensile stress and the consequent exposure of the ADAMST13 cleavage site were revealed by force probe molecular dynamics simulations.[20] To further understand the molecular mechanism underlying the shear force induced cleavage of the VWF A2 domain by ADAMTS13, we carried out structural and functional studies of the A2 domain. We constructed an engineered A2 domain (N1493C/C1670S, ssA2) by introducing an A1/A3-like disulfide bond[20] which allowed us to perform further structural studies. When we solved the crystal structure of the engineered A2 domain, Zhang *et al*. reported the crystal structure of a wild-type A2 domain (wtA2) which provides structural insights into the mechanism of its shear force sensor function[21]. Compared with the wtA2 domain, our ssA2 structure reveals a novel Ca^{2+}-binding site on the α3-β4 loop which is absent in the wtA2 structure. To investigate the potential functional role of the calcium binding in the shear force-dependent cleavage of the VWF A2 domain by ADAMTS13, we preformed molecular dynamics simulations, mutagenesis studies, and in *vitro* biochemical assays. These results show that the binding of Ca^{2+} stabilizes the A2 domain and impedes its unfolding, and consequently, decreases the susceptibility of the A2 domain to ADAMTS13 proteolysis. Our structural and biochemical data together provide new insights into the regulation of VWF cleavage by ADAMTS13 in hemostasis and thrombosis.

Materials and methods

Cloning, expression, and purification of VWF A2 domain

The gene fragment of the VWF A2 domain (residues Leu^{1487}-Gly^{1674}) was amplified from the cDNA of HEK293T cells and inserted into pET22b (Novagen). An engineered A2 domain (ssA2) that contains the N1493C and C1670S mutations was generated to introduce a disulfide bond that links the N- and C-termini of the A2 domain in analogy to that in the

VWF A1 and A3 domains[20].

The ssA2 protein and its mutants were expressed in *E. coli* BL21 (DE3) codon plus cells. The proteins were purified with Ni-NTA affinity chromatography and subsequently gel filtration. The target proteins were concentrated to 15 mg/ml in buffer A (20 mM Tris-HCl, pH 8.0, 300 mM NaCl, 10% glycerol, and 0.1% CHAPS) for crystallization. For inductively coupled plasma atomic emission spectroscopy analysis, the purified ssA2 protein was further dialyzed against buffer B (3 mM Tris-HCl, pH 8.0).

For cleavage assays, the wild-type and mutant wtA2 proteins were expressed in HEK293S GNT1$^-$ cells as described before.[21] The target proteins were purified by Ni-NTA affinity chromatography. VWF73 (residues Asp^{1596}-Arg^{1668}) was shown to be the minimal substrate for ADAMTS13.[22] The VWF73 gene fragment with a C-terminal hexahistidine tag was inserted into pGEX4T1. The wild-type and mutant GST-VWF73 proteins were expressed in *E. coli* BL21 (DE3) codon plus cells and purified by Ni-NTA and subsequently GST affinity chromatography. The purified wtA2 and VWF73 proteins were dialyzed against buffer C (50 mM HEPES, pH 7.4, and 150 mM NaCl) for cleavage assays.

Crystallization, diffraction data collection, and structure determination and refinement

The crystallization experiments were carried out at 4 ^{o}C using the hanging drop vapor diffusion method. The crystals of ssA2 and its mutants were grown in drops containing equal volumes of the protein solution and the crystallization solution (0.1 M sodium citrate, pH 5.2, and 1.6 M $(NH_4)_2SO_4$). The crystals were cryoprotected with the reservoir solution supplemented with 25% glycerol, and were then flash-frozen in liquid nitrogen. X-ray diffraction data were collected at 100 K at beamline 17U of Shanghai Synchrotron Radiation Facility, China at a wave length of 1.0000 Å using a MAR225 detector, and were processed using the HKL2000 suite[23]. The diffraction data statistics are summarized in **Table 1**.

The ssA2 structure was solved using the molecular replacement method implemented in

PHASER[24] with the VWF A3 structure (PDB code 1AO3)[25] as a search model. The initial structure refinement was carried out with CNS[26] and the manual model building was performed with COOT[27]. In the initial difference Fourier maps, it was evident that a disulfide bond forms between Cys1493 and Cys1669, and strong electron density corresponding to a metal ion was detected near the α3-β4 loop (the nomenclature of the secondary structures of ssA2 adopts that of wtA2 by Zhang *et al.*[21]) which was further identified as a Ca^{2+} ion (see Results). The final structure refinement was performed with REFMAC5[28]. The structures of the ssA2 mutants were determined using the ssA2 structure as the starting model. The statistics of the structure refinement and the final structure models are listed in **Table 1**.

Force probe molecular dynamics simulations

Molecular modeling and *in silico* mutagenesis were performed with MOE (2009.10, Chemical Computing Group CCG). A wild-type A2 model (residues 1495 to 1671) was constructed based on the ssA2 structure by mutations of Cys1493 back to Asn and Ser1670 back to Cys and subsequent generation of a vicinal disulfide bridge between Cys1669 and Cys1670. The assigned Ca^{2+} ion was kept or replaced with a water molecule.

All molecular dynamics (MD) simulations and analyses were carried out with the Gromacs suite (Version 3.3.3)[29] and the OPLS all atom force field[30]. For the equilibrium MD simulations, the protein was solvated in dodecahedral boxes with at least 5,500 TIP4p water molecules[31] under periodic boundary conditions. The typical protonation states at pH 7 were chosen for ionizable groups of the protein and the necessary amount of counter-ions (Cl^- and Na^+) were added to ensure a neutral system of physiological ion strength. A temperature of 300 K and a pressure of 1 bar were assumed. The wtA2 models were simulated each for at least 20 ns and up to 40 ns.

For the force probe MD, the systems were solvated in 19 nm long rectangular boxes each containing about 20,000 water molecules. Harmonic springs were attached to the

terminal C_α atoms with spring constants of 500 kJ/(mol·nm²) and then moved away from each other with a velocity of 1.25 nm/ns and hence each of the simulations spanned about 26 ns. To keep the system size (simulation box size) reasonable, the force probe MD simulations were split into two parts. In the beginning, the whole wtA2 domain (residues 1495 to 1671) was simulated until unfolding of the C-terminal secondary structure elements α6, β6, and α5 was completed. Subsequently, the unfolded region (residues 1634 to 1671) was removed and the force probe MD simulations were continued with the truncated fragment.

A2 cleavage assays

The *in vitro* cleavage assays of the wtA2 and GST-VWF73 proteins include pre-incubation of the proteins with urea at different concentrations of Ca^{2+} (step I), followed by administration of ADAMST13 for the A2 cleavage (step II). In step I, 200 μg/ml A2 protein in the assay buffer (50 mM HEPES, pH 7.5, 150 mM NaCl, 50 μM $ZnCl_2$, and 0.1% BSA) was incubated at 37 ^oC for 2 hours with different concentrations of urea (1.92 M, 2.56 M, 3.20 M, and 3.84 M) and Ca^{2+} (0 mM, 2.5 mM, and 5.0 mM). For the VWF73 substrates, urea was not added. In step2, for each reaction, 5 μl of the pre-incubated A2 protein in the assay buffer and 5 μl of 20 μg/ml ADAMTS13 (R&D Systems) in 50 mM Tris-HCl (pH 8.5) were mixed and then incubated at 37 ^oC for one hour, with or without adjustment of the Ca^{2+} concentration. In some assays, step I was omitted, and 5 μl of the ssA2 protein in the assay buffer containing different concentrations of urea and Ca^{2+} were incubated with 5 μl of the diluted ADAMTS13 at 37 ^oC for three hours. The cleaved C-terminal fragments of the A2 proteins and the intact A2 proteins were detected using Western blotting with specific antibodies anti-A2C (R&D Systems) and anti-His (Tiangen), respectively. All experiments were performed at least three times.

Results

Crystal structure of VWF A2 domain

The wild-type (wtA2) protein we expressed with the *E. coli* expression system was insoluble, and the refolded wtA2 did not show homogeneity and failed to produce any crystal. Thus, an engineered A2 domain (ssA2) was generated by introducing two mutations (N1493C and C1670S) to form a disulfide bond between the N- and C-termini analogous to that in the VWF A1 and A3 domains[20] which allowed further structural studies.

The crystals of ssA2 belong to space group $P6_5$ (**Table 1**) which is different from that of wtA2 ($P2_1$)[21]. The asymmetric unit contains one ssA2 molecule, corresponding to a Matthews coefficient of 2.3 $Å^3$/Da and a solvent content of 46%. The ssA2 structure was determined at 1.9 Å resolution, and has been refined to an R factor of 20.1% and a free R factor of 23.1% (**Table 1**). The ssA2 structure assumes a typical Rossmann fold and is very similar to the wtA2 structure with an RMSD of 1.0 Å for all C_α atoms (**Figures 1A and 1B**). It is noteworthy that as observed in the wtA2 structure (PDB code 3GXB) [21] Pro1645 takes a cis configuration.

A novel Ca^{2+}-binding site

The only major conformational difference between the ssA2 and wtA2 structures occurs in the region (residues 1591-1602) connecting α3 and β4. This region forms a short 3_{10} helix in wtA2 but a loop in ssA2 (**Figure 1B**). The disulfide bond between Cys1493 and Cys1669 does not cause any notable conformational change in the nearby regions and hence is unrelated to the observed conformational change of the α3-β4 loop (supplementary **Figure S1A**). Intriguingly, a metal ion is bound at this loop with evident electron density (supplementary **Figure S1B**). It is coordinated in a octahedral geometry by six ligands, namely the main-chain carbonyls of Arg1597 (2.3 Å) and Ala1600 (2.3 Å), the side-chain carboxyl of Asp1498 (2.3 Å) and Asp1596 (2.4 Å), the side-chain carbonyl of Asn1602 (2.3

Å), and a water molecule (2.4 Å) (**Figure 1C)**. The metal ion might be a Ca^{2+} ion as this geometry is a typical calcium binding geometry.[32] Interestingly, at the equivalent site of wtA2, a molecule was also observed with six coordinating ligands (**Figure 1D**), which was assigned as a water molecule (see discussion later).

To identify the type of the metal ion, we performed inductively coupled plasma atomic emission spectroscopy analyses of the protein solution and the buffer. The results show a higher content of calcium ions (0.0042% *vs.* 0.0011%) and zinc ions (0.0013% *vs.* 0.0002%) in the protein solution than in the buffer alone **(Table 2)**, suggesting that the bound metal ion might be a Ca^{2+} or Zn^{2+} ion. For further verification, we collected the anomalous dispersion data at the peak wavelengths of zinc (1.28 Å) and Ni^{2+} (1.49 Å), and the most commonly used wavelength for calcium (1.77 Å), respectively. Evident anomalous signal was only detected at the metal-binding site at the wavelength of 1.77 Å (supplementary Figure S2A), indicating that the bound metal ion is a Ca^{2+} ion rather than a Zn^{2+} or Ni^{2+}. Since no Ca^{2+} and Zn^{2+} ions were added in the crystallization solution, it is most likely that the bound Ca^{2+} ion is co-purified with the protein from the expression system and the trace of Zn^{2+} ions in the protein solution are non-specifically bound to the C-terminal hexahistidine tag.

To investigate whether mutations of residues at the metal-binding site would impede the calcium binding, the crystal structures of the D1596A, N1602A, and D1596A/N1602A mutants of ssA2 were determined. In all of these mutant structures, the region encompassing residues 1591-1602 still assumes a loop conformation similar to that in the intact ssA2, and there is evident electron density at the metal-binding site corresponding to a bound metal ion. However, due to the loss of ligand(s), the coordination geometries of the metal ion are distorted with a five-coordination geometry in the D1596A and N1602A mutants and a four-coordination geometry in the D1596A/N1602A mutant (**Figure 1E-G**). The coordination bond lengths are much longer than those in the ssA2 structure but similar to those in the

wtA2 structure (**Figure 1E-G** and supplementary **Table S1,** see discussion later). In addition, we collected the anomalous dispersion data at the wavelength of 1.77 Å for all of these mutants but no anomalous signal was observed, indicating that the bound ions in the mutants are unlikely Ca^{2+}. These results suggest that mutations of Asp1596 and Asn1602 impair the ability of ssA2 to bind Ca^{2+}.

Calcium binding impedes the unfolding of the A2 domain

To explore the functional role of Ca^{2+} binding, we conducted simulation studies to examine the effect of Ca^{2+} binding on the force required for the unfolding of the A2 domain. Based on the ssA2 structure, we constructed a wtA2 model with removal of the engineered disulfide bond and subsequent generation of a vicinal disulfide bridge between Cys1669 and Cys1670 as observed in the wtA2 structure. The derived wtA2 model was stable in equilibrium MD simulations and particularly, the Ca^{2+} binding site remains intact and the ion stays in place, again indicating that the observed loop conformation of the α3-β4 region and the Ca^{2+} binding are unrelated to the engineered disulfide bond. This model was then subjected to force probe MD simulations with or without Ca^{2+} bound.

The force probe MD simulation results of the wtA2 model were compared with those of the wtA2 structure[20]. For the initial unfolding of the C-terminal part (α6, β6, and α5), the trajectories of the wtA2 model with and without Ca^{2+} are similar, which also resemble those of the wtA2 structure[20]. For the unfolding of the central β-sheet (strands β5 and β4), although the force profiles are different for the wtA2 model with a higher force needed to unfold β4, in the absence of Ca^{2+}, the force required for the unfolding of the central β-sheet in the simulations of the wtA2 model is almost the same (approximately 1000 pN) (**Figure 2A, left panel**) in this study and in the previous report[20]. Intriguingly, when Ca^{2+} is bound, the force significantly increases to 1250 pN for the unfolding of strand β4 (**Figure 2A, right panel**), indicating that the interplay between Ca^{2+} and the involved residues at the metal-binding site

impedes the unfolding of the A2 domain, in particular the detachment of β4 from the remaining protein core. Thus, the binding of Ca^{2+} renders A2 more resistant against pulling forces as present in the shear flow of blood.

When Ca^{2+} is bound, the trajectories of the unfolding of the β4 strand are also different with the force peak being split into 3 sub-peaks that represent breakage of inter-strand interactions within the central β-sheet, the associated movement of the central β-sheet, and the stepwise disruption of the Ca^{2+}-binding site. At the beginning, Asn1602 is pulled away from the Ca^{2+}-binding site followed by the movement of β4 (**Figure 2B**, **snapshots I and II**). After the second sub-peak, the Ca^{2+} ion is only coordinated by Asp1596 and Asp1498 (**Figure 2B**, **snapshot III**). Finally, the Ca^{2+}-binding site is demolished and β4 is completely unfolded (**Figure 2B**, **snapshot IV**).

Calcium binding protects A2 from cleavage by ADAMTS13

As the unfolding of the A2 domain is essential for the cleavage of VWF by ADAMTS13, we reason that the binding of Ca^{2+} would have an impact on VWF cleavage. This hypothesis was examined using *in vitro* biochemical assays which include pre-treatment of the A2 substrate with urea to facilitate the unfolding process (step I) followed by the proteolysis of A2 by ADAMTS13 (step II), using the wtA2 proteins which were expressed in HEK293S $GNT1^-$ cells with glycosylation (see discussion later) but not the engineered ssA2 proteins as substrates. To investigate the effect of Ca^{2+} on the unfolding process only, varying concentrations of Ca^{2+} (0 mM, 2.5 mM, and 5.0 mM) were added at step I, while the Ca^{2+} concentration was adjusted to the same (2.5 mM which is within the normal range of blood calcium concentration) at step II. As shown in **Figure 3A**, in the presence of high concentration of urea, the wtA2 protein was cleaved by ADAMTS13; however, supplementation of Ca^{2+} at the concentration of either 2.5 mM or 5.0 mM during step I significantly suppressed the process, indicating that the Ca^{2+} binding indeed impedes the

unfolding of wtA2 and consequently its cleavage by ADAMTS13 (**Figure 3A**).

On the other hand, if Ca^{2+} exerts a protective function via the Ca^{2+}-binding site, disruption or a lack of the Ca^{2+}-binding site would abolish the protective role of Ca^{2+}. VWF73 (corresponding to residues Asp^{1596} to Arg^{1668} of the A2 domain) is the minimal substrate of ADAMTS13 which is presumably unfolded and susceptible to the cleavage by ADAMTS13 without shear stress or chaotropic agents[22]. Supposedly it does not have a Ca^{2+}-binding site due to the absence of both Asp1498 and a defined structure. Consistently, pre-treatment of VWF73 with Ca^{2+} had no effect on the cleavage of this fragment (**Figure 3B**), indicating the necessity of an intact Ca^{2+}-binding site for the protection of VWF by Ca^{2+} from ADAMTS13 cleavage.

The metalloprotease ADAMTS13 requires Zn^{2+} (ref. 33) or Ca^{2+} (refs. 7 and 14) for its activity, and it has been reported that the activity of ADAMTS13 is enhanced about 160-fold at 5 μM Ca^{2+}.[34] Thus, Ca^{2+} may have two opposing effects on VWF cleavage, namely stabilization of the A2 domain and enhancement of the enzymatic activity of ADAMTS13. Given that the physiological concentration of Ca^{2+} remains stable, this combined effect of Ca^{2+} was examined with the Ca^{2+} concentration kept unchanged during step I (corresponding to the unfolding process) and step II (corresponding to the proteolytic process). As shown in **Figure 3C**, the results show a similar trend as observed in **Figure 3A**, again demonstrating that the presence of Ca^{2+} leads to decreased susceptibility of the VWF A2 domain. Considering that the VWF unfolding and ADAMTS13 cleavage occur in the same environment *in vivo*, the A2 cleavage assay was further modified so that step I and step II were no longer separated, and the A2 unfolding and ADAMTS13 cleavage were carried out under the same condition (**Figure 3D**). The results were very similar to those presented in **Figure 3C**, again supporting a protective role of Ca^{2+} in VWF proteolysis.

Mutations at the Ca^{2+}-binding site impair the protective effect of Ca^{2+} on A2 cleavage

To further investigate the functional role of the Ca^{2+} binding in the protection of the A2 domain, the wtA2 mutants (D1596A, D1498A, R1597W, and N1602A) which carry point mutations of the key residues at the Ca^{2+}-binding site were analyzed with *in vitro* cleavage assays. At all the three urea concentrations examined, the cleavage of the D1596A mutant appears independent of the calcium concentrations, implying that the side-chain carboxyl is required for exertion of the protective function of Ca^{2+} binding (**Figure 4A**). This finding agrees well with the critical role of Asp1596 shown by the structural investigations on ssA2 and its D1596A mutant.

The rest of the mutants were examined with two-step ADAMTS13 cleavage assays with a fixed urea concentration (2.56 M) in step I. The D1498A mutant shows a dramatically increased susceptibility to ADAMTS13, and the presence of high Ca^{2+} concentration shows no effect on the protection of the A2 unfolding in step I (**Figure 4B**). Besides its participation in the formation of the Ca^{2+}-binding site, the side-chain carboxyl group of Asp1498 forms a salt bridge with the side-chain amino group of Arg1597 which stabilizes the position of Arg1597. Thus, mutation of Asp1498 to Ala might lead to instability of this region, which probably facilitates the unfolding of the A2 domain, partially explaining the substantially increased susceptibility of this mutant. The type 2A VWD associated R1597W mutant shows similar levels of susceptibility to ADAMTS13 in the presence and absence of Ca^{2+} in step I (**Figure 4B**), indicating that the Ca^{2+} protection of A2 cleavage is abolished by the R1597W mutation. Such effect might be resulted from a change in the configuration of its main-chain carbonyl due to the introduction of a bulky side chain and the loss of the salt-bridging interaction with Asp1498 and the consequent loss or decrease of coordination with Ca^{2+}. Intriguingly, the N1602A mutation led to resistance of A2 to the digestion by ADAMTS13 (**Figures 4B**, see discussion later).

The mutations D1596A, N1602A, and R1597W were also investigated for the

ADAMTS13 minimal substrate VWF73. As expected, mutations D1596A and R1597W exhibit no effect on the susceptibility of VWF73 to ADAMTS13 proteolysis (**Figure 4C**). It is intriguing to observe that mutation N1602A also led to resistance of the VWF73 fragment to the proteolysis (**Figures 4C**), although the protective effect of Ca^{2+} might be lost due to the disruption of the Ca^{2+}-binding site by the N1602A mutation. It has been shown that the range of the recognized cleavage site for ADAMTS13 encompasses residues Arg1597 to Ile1623.[35] Our results indicate a critical role of Asn1602 for cleavage of VWF by ADAMTS13 probably due to its proximity to the cleavage site of Tyr1605-Met1606. The detailed functional role(s) of Asn1602 need to be investigated further.

Discussion

With structural, computational, and biochemical data, we reveal a novel Ca^{2+}-binding site at the A2 domain of VWF and show that Ca^{2+} binding at this site protects its unfolding and subsequent proteolysis by ADAMTS13. The VWF A2 domain shares structural similarities with other von Willebrand factor A (VWA) domains.[25,36,37] Although binding of metal ions has been reported in VWA domains[37], this is the first time that a metal binding site is observed in A domains of VWF, which is different from the metal-binding site of other VWA domains.

Comparison of the equivalent sites in the ssA2 and wtA2 structures shows that one major difference lies in the position and configuration of Asp1596 (**Figures 1C and 1D**). In the ssA2 structure, Asp1596 is located in the α3-β4 loop and points its side chain towards inside to coordinate the bound Ca^{2+} ion; whereas in the wtA2 structure, Asp1596 resides in the 3_{10}-helix and the side chain points away from the tentative Ca^{2+}-binding site[38]. Despite the differences, in the wtA2 structure a molecule is also detected at the site equivalent to the Ca^{2+}-binding site of ssA2, forming six coordination bonds with the surrounding residues and

water molecules in a geometry similar to that in our ssA2 structure. However, the bond lengths are much longer than those in the ssA2 structure (2.7-3.3 Å *vs*. 2.3-2.4 Å). Intriguingly, in the D1596A mutant of ssA2, with loss of the coordination of Asp1596, the Ca^{2+}-binding site is partially assembled as in the wtA2 structure, and similarly, a molecule is bound with longer bond lengths (2.5-2.9 Å). As this molecule is not a Ca^{2+} ion based on the anomalous dispersion result, in analogy, the molecule bound at the same position of wtA2 is unlikely a Ca^{2+} ion, implying that the partially assembled site is insufficient for Ca^{2+} binding. It is noteworthy that glycosylation of wtA2 occurs at Gln1515 and Gln1574 of the A2 domain of VWF, and mutation of Gln1574 which prevents its glycosylation leads to increased susceptibility of VWF and VWF A2 to ADAMTS13 proteolysis.[39] Indeed, in the wtA2 structure, N-linked glycans are observed at Gln1515 and Gly1574. The glycosylation sites and the Ca^{2+}-binding site are located on opposite sides of the A2 domain, and the glycosylation is unlikely to affect the assembly of the Ca^{2+}-binding site (supplementary **Figure S3**).

To investigate whether the differences in the conformation of the α3-β4 region and Ca^{2+} binding between the wtA2 and ssA2 structures are due to the different crystallization conditions, we explored the possibilities of obtaining a wtA2 structure with and an ssA2 structure without a Ca^{2+} ion bound. Attempts to grow crystals of wtA2 under the crystallization condition reported here and crystals of ssA2 under the condition reported by Zhang *et al.*[21] were unsuccessful. Instead, we obtained crystals of wtA2 from both the co-crystallization and soaking experiments under the same crystallization condition as used by Zhang *et al.*[21] with supplementation of 10 mM $CaCl_2$, and crystals of the ssA2 protein treated with 10 mM EDTA under the crystallization condition reported here. No calcium signal was detected in anomalous dispersion diffraction data of these crystals (data not shown). In the derived wtA2 structures, the α3-β4 region assumes the same 3_{10}-helical

conformation with a molecule bound at the metal-binding site in a way similar to that in the wtA2 structure (data not shown), indicating that the α-helical conformation of the α3-β4 region and the incapability of binding a Ca^{2+} are intrinsic properties of the wtA2 structure under the corresponding crystallization condition. On the other hand, in the structure of EDTA-treated ssA2 determined at 2.0 Å resolution, the Ca^{2+}-binding site is almost identical to that in the structure of ssA2 in complex with Ca^{2+} (supplementary **Figure S2B**) although no Ca^{2+} is bound, implicating that the formation of the binding site in ssA2 is not induced by Ca^{2+}, but occurs naturally under the crystallization condition.

These results indicate that the loop conformation of the α3-β4 region and the capability of binding a Ca^{2+} are intrinsic properties of the ssA2 structure under the crystallization condition reported in this study, and the observed differences between the wtA2 and ssA2 structures might result from the different crystallization conditions. Analysis of the crystal packing of the two crystal forms reveals that the α3-β4 region is exposed on the solvent accessible surface in both structures and is engaged in the interactions with the symmetry-related molecules in the wtA2 (supplementary **Figure S4A**) but not ssA2 structure. Moreover, superposition of the ssA2 structure onto the wtA2 structure shows that in the crystal packing of wtA2, the α3-β4 region of the ssA2 would clash with the symmetry-related molecule (supplementary **Figure S4B**). Therefore, the crystal packing in the wtA2 structure hinders the α3-β4 region from forming a loop structure and hence prevents complete assembly of the Ca^{2+}-binding site. In solution, it is plausible that the α3-β4 region of VWF A2 might have a high flexibility with the 3_{10}-helical conformation seen in the wtA2 structure and the loop conformation seen in the ssA2 structure as two quasi-stable conformations, which have been independently captured under different crystallization conditions.

Intriguingly, it is recently reported that there is an intermediate unfolded state of A2 which shows unfolding of the C-terminal region up to the β4 strand.[19] Out of the five residues

involved in the formation of the Ca^{2+}-binding site identified in this study, four (Asp1596, Arg1597, Ala1600, and Asn1602) are located in the C-terminal region of the α3-β4 loop which immediately flanks the β4 strand (supplementary **Figure S5**). Based on the crystal structure of the catalytic domain of ADAMTS5[40], we constructed a model of ADAMTS13 which shows that the active site of the enzyme is a narrow and deep groove (unpublished data), suggesting that the β4 strand needs to be displaced and inserted into the groove for ADAMTS13 cleavage. The displacement of the β4 strand would require the conformational change of the α3-β4 loop and very likely the disruption of the Ca^{2+}-binding site as well, which implies that Ca^{2+} exerts its protective role through stabilization of the α3-β4 loop and hence restraint of the β4 strand.

Protein Data Bank accession codes

The structures of ssA2 and its D1596A, N1602A and D1596A/N1602A mutants have been deposited with the RCSB Protein Data Bank under accession codes 3PPV, 3PPW, 3PPX, and 3PPY, respectively.

Acknowledgments

We thank the staff members at SSRF, China for technical support in diffraction data collection. We thank Professors Xiaohui Zhang, Jianfeng Chen, and Reinhard Schneppenheim for inspiring discussions. This work was supported by grants from the Ministry of Science and Technology of China (2007CB914302 and 2011CB966301), the National Natural Science Foundation of China (30730028), the Chinese Academy of Sciences (KSCX2-YW-R-107 and SIBS2008002), and Klaus Tschira foundation. CB is grateful for a Feodor Lynen fellowship by the Alexander von Humboldt Foundation.

Authorship

MZ and XD carried out the structural and biochemical studies and drafted the manuscript. CB and FG conceived the MD simulation studies. CB carried out the MD simulation studies and participated in the drafting of the manuscript. HC and XL participated in the biochemical studies. YZ and TAS provided the initial wild-type A2 domain sample and crystals. CZ participated in the data analysis and drafting of the manuscript. JD conceived of the study, participated in the experimental design and coordination, and wrote the manuscript.

Disclosure of Conflict of Interest: The authors declare no competing financial interests.

References

1. Sadler JE. Biochemistry and genetics of von Willebrand factor. *Annu Rev Biochem*. 1998;67:395-424.
2. Reininger AJ. Function of von Willebrand factor in haemostasis and thrombosis. *Haemophilia*. 2008;14 (Suppl 5):11-26.
3. Ruggeri ZM. Structure and function of von Willebrand factor. *Thromb Haemost*. 1999;82(2):576-584.
4. Sadler JE. von Willebrand factor: two sides of a coin. *J Thromb Haemost*. 2005;3(8):1702-1709.
5. Levy GG, Nichols WC, Lian EC, et al. Mutations in a member of the ADAMTS gene family cause thrombotic thrombocytopenic purpura. *Nature*. 2001;413(6855):488-494.
6. Batlle J, Lopez-Fernandez MF, Lopez-Borrasca A, et al. Proteolytic degradation of von Willebrand factor after DDAVP administration in normal individuals. *Blood*. 1987;70(1):173-176.
7. Furlan M, Robles R, Lammle B. Partial purification and characterization of a protease from human plasma cleaving von Willebrand factor to fragments produced by in vivo proteolysis. *Blood*. 1996;87(10):4223-4234.
8. Sadler JE. A new name in thrombosis, ADAMTS13. *Proc Natl Acad Sci U S A*. 2002;99(18):11552-11554.
9. Dent JA, Berkowitz SD, Ware J, Kasper CK, Ruggeri ZM. Identification of a cleavage site directing the immunochemical detection of molecular abnormalities in type IIA von Willebrand factor. *Proc Natl Acad Sci U S A*. 1990;87(16):6306-6310.
10. Sutherland JJ, O'Brien LA, Lillicrap D, Weaver DF. Molecular modeling of the von Willebrand factor A2 Domain and the effects of associated type 2A von Willebrand disease mutations. *J Mol Model*. 2004;10(4):259-270.
11. Tsai HM, Sussman, II, Nagel RL. Shear stress enhances the proteolysis of von Willebrand factor in normal plasma. *Blood*. 1994;83(8):2171-2179.
12. Schneider SW, Nuschele S, Wixforth A, et al. Shear-induced unfolding triggers adhesion of von Willebrand factor fibers. *Proc Natl Acad Sci U S A*. 2007;104(19):7899-7903.
13. Furlan M. Von Willebrand factor: molecular size and functional activity. *Ann Hematol*. 1996;72(6):341-348.
14. Tsai HM. Physiologic cleavage of von Willebrand factor by a plasma protease is dependent on its conformation and requires calcium ion. *Blood*. 1996;87(10):4235-4244.
15. Dong JF, Moake JL, Nolasco L, et al. ADAMTS-13 rapidly cleaves newly secreted ultralarge von Willebrand factor multimers on the endothelial surface under flowing conditions. *Blood*. 2002;100(12):4033-4039.
16. Tsai HM. Shear stress and von Willebrand factor in health and disease. *Semin Thromb Hemost*. 2003;29(5):479-488.
17. Sadler JE. New concepts in von Willebrand disease. *Annu Rev Med*. 2005;56:173-191.
18. Hassenpflug WA, Budde U, Obser T, et al. Impact of mutations in the von Willebrand factor A2 domain on ADAMTS13-dependent proteolysis. *Blood*. 2006;107(6):2339-2345.
19. Zhang X, Halvorsen K, Zhang CZ, Wong WP, Springer TA. Mechanoenzymatic cleavage of the ultralarge vascular protein von Willebrand factor. *Science*. 2009;324(5932):1330-1334.
20. Baldauf C, Schneppenheim R, Stacklies W, et al. Shear-induced unfolding activates von Willebrand factor A2 domain for proteolysis. *J Thromb Haemost*. 2009;7(12):2096-2105.
21. Zhang Q, Zhou YF, Zhang CZ, Zhang X, Lu C, Springer TA. Structural specializations of A2, a force-sensing domain in the ultralarge vascular protein von Willebrand factor.

Proc Natl Acad Sci U S A. 2009;106(23):9226-9231.
22. Kokame K, Matsumoto M, Fujimura Y, Miyata T. VWF73, a region from D1596 to R1668 of von Willebrand factor, provides a minimal substrate for ADAMTS-13. *Blood*. 2004;103(2):607-612.
23. Otwinowski Z, Minor W. Processing of X-ray Diffraction Data Collected in Oscillation Mode. *Methods in Enzymology*. 1997;276:307-326.
24. McCoy AJ. Solving structures of protein complexes by molecular replacement with Phaser. *Acta Crystallogr*. 2007;D63(Pt 1):32-41.
25. Huizinga EG, Martijn van der Plas R, Kroon J, Sixma JJ, Gros P. Crystal structure of the A3 domain of human von Willebrand factor: implications for collagen binding. *Structure*. 1997;5(9):1147-1156.
26. Brunger AT, Adams PD, Clore GM, et al. Crystallography & NMR system: A new software suite for macromolecular structure determination. *Acta Crystallogr*. 1998;D54(Pt 5):905-921.
27. Emsley P, Cowtan K. Coot: model-building tools for molecular graphics. *Acta Crystallogr*. 2004;D60(Pt 12):2126-2132.
28. Murshudov GN, Vagin AA, Dodson EJ. Refinement of macromolecular structures by the maximum-likelihood method. *Acta Crystallogr*. 1997;D53(Pt 3):240-255.
29. Van Der Spoel D, Lindahl E, Hess B, Groenhof G, Mark AE, Berendsen HJ. GROMACS: fast, flexible, and free. *J Comput Chem*. 2005;26(16):1701-1718.
30. Jorgensen WL, Ulmschneider JP, Tirado-Rives J. Free energies of hydration from a generalized Born model and an ALL-atom force field. *J Phys Chem B*. 2004;108:16264-16270.
31. Lawrence CP, Skinner JL. Flexible TIP4P model for molecular dynamics simulation of liquid water. *Chem Phys Lett*. 2003;372:842-847.
32. Harding MM. Geometry of metal-ligand interactions in proteins. *Acta Crystallogr*. 2001;D57(Pt 3):401-411.
33. Tsai HM, Sussman, II, Ginsburg D, Lankhof H, Sixma JJ, Nagel RL. Proteolytic cleavage of recombinant type 2A von Willebrand factor mutants R834W and R834Q: inhibition by doxycycline and by monoclonal antibody VP-1. *Blood*. 1997;89(6):1954-1962.
34. Anderson PJ, Kokame K, Sadler JE. Zinc and calcium ions cooperatively modulate ADAMTS13 activity. *J Biol Chem*. 2006;281(2):850-857.
35. Gao W, Anderson PJ, Sadler JE. Extensive contacts between ADAMTS13 exosites and von Willebrand factor domain A2 contribute to substrate specificity. *Blood*. 2008;112(5):1713-1719.
36. Emsley J, Cruz M, Handin R, Liddington R. Crystal structure of the von Willebrand Factor A1 domain and implications for the binding of platelet glycoprotein Ib. *J Biol Chem*. 1998;273(17):10396-10401.
37. Springer TA. Complement and the multifaceted functions of VWA and integrin I domains. *Structure*. 2006;14(11):1611-1616.
38. Harding MM. Metal-ligand geometry relevant to proteins and in proteins: sodium and potassium. *Acta Crystallogr*. 2002;D58(Pt 5):872-874.
39. McKinnon TA, Chion AC, Millington AJ, Lane DA, Laffan MA. N-linked glycosylation of VWF modulates its interaction with ADAMTS13. *Blood*. 2008;111(6):3042-3049.
40. Mosyak L, Georgiadis K, Shane T, et al. Crystal structures of the two major aggrecan degrading enzymes, ADAMTS4 and ADAMTS5. *Protein Sci*. 2008;17(1):16-21.

Table 1. Statistics of X-ray diffraction data and structure refinement

	ssA2	ssA2-D1596A	ssA2-N1602A	ssA2-D1596A/N1602A
PDB code	3PPV	3PPW	3PPX	3PPY
Diffraction data				
Space group	$P6_5$	$P6_5$	$P6_5$	$P6_5$
Cell parameters				
$a = b$ / c (Å)	69.8 / 73.6	72.1 / 76.3	72.1 / 76.3	72.5 / 76.3
Resolution range (Å)	50.0-1.9 (1.97-1.90)[a]	50.0-1.9 (1.97-1.90)	50.0-1.9 (1.97-1.90)	50.0-2.0 (2.07-2.00)
Observed reflections	132,324	72,418	95,704	101,783
Unique reflections (I/σ(I)> 0)	15,647	17,621	17,507	15,351
Average redundancy	8.5 (4.9)	4.1 (3.1)	5.5 (4.2)	6.6 (4.4)
I/σ(I)	20.9 (2.5)	23.1 (6.7)	16.8 (3.6)	17.3 (3.4)
Completeness (%)	97.0 (87.5)	99.0 (97.8)	98.2 (82.5)	99.3 (96.6)
R_{merge} (%) [b]	10.3 (46.9)	5.8 (27.0)	12.2 (43.6)	12.3 (40.9)
Refinement and structure model				
Reflections (Fo>0σ(Fo))	15,645	17,597	17,506	15,335
Working set	14,864	16,707	16,615	14,552
Free R set	781	890	891	783
R factor (%)[c]	20.1 (26.5)	21.0 (29.1)	20.6 (27.0)	20.1 (23.6)
Free *R* factor (%)[c]	23.1 (36.9)	23.6 (33.7)	23.7 (28.0)	23.2 (24.6)
Subunits/ASU	1	1	1	1
Average B factor (Å^2)	23.0	15.4	16.7	16.8
Protein main-chain atoms	20.0	13.4	15.3	14.8
Protein side-chain atoms	24.0	14.4	16.3	16.8
RMSD bond lengths (Å)	0.006	0.006	0.006	0.006
RMSD bond angles (°)	1.1	1.1	1.1	1.1
Luzzati positional error (Å)	0.228	0.237	0.227	0.222
Ramachandran plot (%)				
Most favored regions	91.1	93.0	93.0	92.5
Allowed regions	8.3	6.4	6.4	6.9
Generously allowed regions	0.6	0.6	0.6	0.6

[a] Numbers in parentheses refer to the highest resolution shell.

[b] $R_{merge} = \sum_{hkl} \sum_i \left| I_i(hkl)_i - \langle I(hkl) \rangle \right| / \sum_{hkl} \sum_i I_i(hkl)$.

[c] R factor = $\Sigma ||F_o|-|F_c|| / \Sigma |F_o|$.

Table 2. ICP-AES analysis results

Metal	Protein solution (%)	Buffer (%)
Ca	0.0042	0.0011
Zn	0.0013	0.0002
Cu	0.0002	0.0002

Figure legends

Figure 1. Structure of ssA2. (A) Two views of the overall structure of ssA2. The A2 domain forms a compact structure with the Tyr1605-Met1606 cleavage site being buried. Residues Tyr1605 and Met1606 are shown with stick-and-ball models and colored in blue. The region of ssA2 N-terminal to the cleavage site is colored in green and that C-terminal to the site in salmon. The bound Ca^{2+} ion is shown as a golden sphere. The secondary structure elements of ssA2 are labeled. **(B)** Structural comparison of ssA2 (cyan) and wtA2 (pink, PDB code 3GXB). The major structural difference occurs in the α3-β4 region. The α3-β4 region is labeled and enclosed in a circle. **(C)** The Ca^{2+}-binding site of ssA2. The surrounding residues are shown with ball-and-stick models. The coordination bonds between Ca^{2+} and the ligands are indicated with dashed lines and the bond lengths (Å) are marked. **(D-G**) The equivalent sites in wtA2 and the ssA2 mutants. The wtA2 protein (**D**) is colored in magenta, and those of the D1596A (**E**), N1602A (**F**), and D1596A/N1602A (**G**) mutants of ssA2 are colored in white, blue, and orange, respectively. In each of these structures, a molecule (wheat) is bound at this site, however, in a geometry different from that of ssA2.

Figure 2. Force probe MD simulations of a wild-type A2 model with or without a Ca^{2+} bound at the metal-binding site. (A) Force profiles of force probe MD simulations of the wtA2 model. The α3-β4 region adopts a loop conformation with or without a Ca^{2+} ion bound at the site equivalent to the Ca^{2+}-binding site of ssA2. The Ca^{2+} ion is replaced with a water molecule (left panel) or kept at the binding site (right panel). (**B**) Selected snapshots of the trajectory of force probe MD simulations of the wtA2 model bound with a Ca^{2+} ion. For the A2 domain, the α-helices are colored in pink, the β strands in yellow, and the α3-β4 loop in cyan. The β4 strand is marked. The residues which participate in the formation of the Ca^{2+}-binding site are shown with ball-and-stick models and labeled. The bound Ca^{2+} is shown as a golden sphere.

Figure 3. Effect of Ca^{2+} binding on the A2 cleavage by ADAMTS13. (A) Examination of the protective effect of Ca^{2+} with two-step ADAMST13 cleavage assays. In step I, the wtA2 protein was denatured under different urea concentrations and calcium was supplemented as indicated. In step II, the Ca^{2+} concentration was adjusted to 2.5 mM. The cleaved and intact A2 proteins were detected with western blotting using the specific antibodies. **(B)** Examination of the effect of Ca^{2+} on the proteolysis of the GST-VWF73 proteins by ADAMTS13. No urea was added in step I. **(C)** Examination of the effect of Ca^{2+} on the proteolysis of the wtA2 protein by ADAMTS13 without adjustment of the calcium concentration in step II. **(D)** Examination of the effect of Ca^{2+} ion on the proteolysis of wtA2 by ADAMTS13 with one-step assays.

Figure 4. Effect of mutations at the Ca^{2+}-binding site on the A2 cleavage by ADAMTS13. **(A)** Examination of the effect of the D1596A mutation on Ca^{2+} protection of A2. In step I, the D1596A mutant A2 was denatured under different urea concentrations and calcium was supplemented as indicated. In step II, the Ca^{2+} concentration was adjusted to 2.5 mM. The cleaved and intact proteins were detected with western blotting using the specific antibodies. **(B)** Examination of the effect of the D1498A, R1597W, and N1602A mutations on Ca^{2+} protection of A2. In step I, 2.56 M urea was added. **(C)** Examination of the effect of the D1498A, R1597W, and N1602A mutations on the proteolysis of GST-VWF73 by ADAMTS13. No urea was added in step I, and the Ca^{2+} concentration was 2.5 mM in both steps.

Figure 1

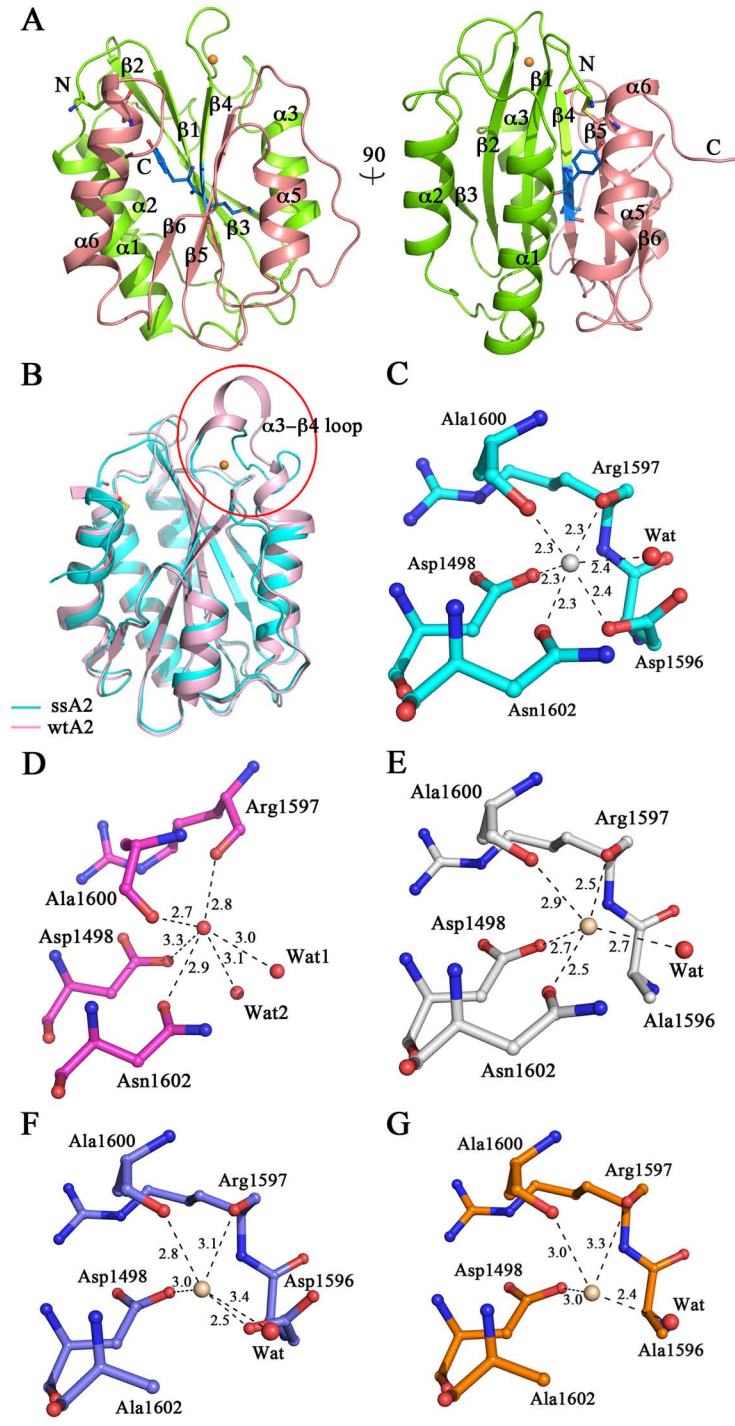
A
N
β2
β1
β4
α3
C
α2
α5
α6
α1
β6
β3
β5
90
N
β1
α6
α3
β4
β5
C
β2
α2
β3
α5
β6
α1
B
α3–β4 loop
ssA2
wtA2
C
Ala1600
Arg1597
Wat
Asp1498
Asp1596
Asn1602
2.3
2.4
D
Arg1597
Ala1600
Asp1498
Wat1
Wat2
Asn1602
2.7
2.8
3.3
3.0
3.1
2.9
E
Ala1600
Arg1597
Asp1498
Wat
Ala1596
Asn1602
2.9
2.5
2.7
F
Ala1600
Arg1597
Asp1498
Asp1596
Wat
Ala1602
2.8
3.1
3.0
3.4
2.5
G
Ala1600
Arg1597
Asp1498
Wat
Ala1596
Ala1602
3.0
3.3
2.4

Figure 2

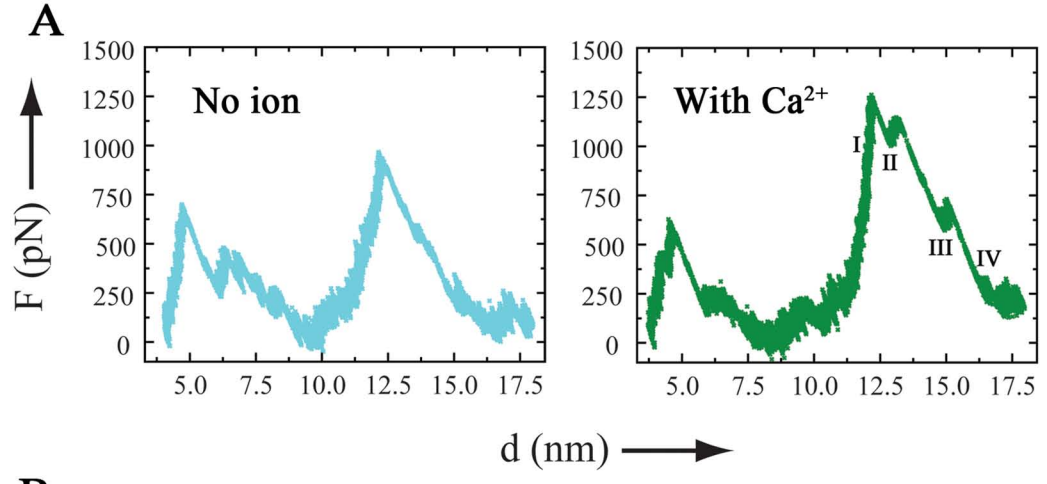
A
No ion
With Ca2+
I
II
III
IV
F (pN)
d (nm)
1500
1250
1000
750
500
250
0
5.0
7.5
10.0
12.5
15.0
17.5

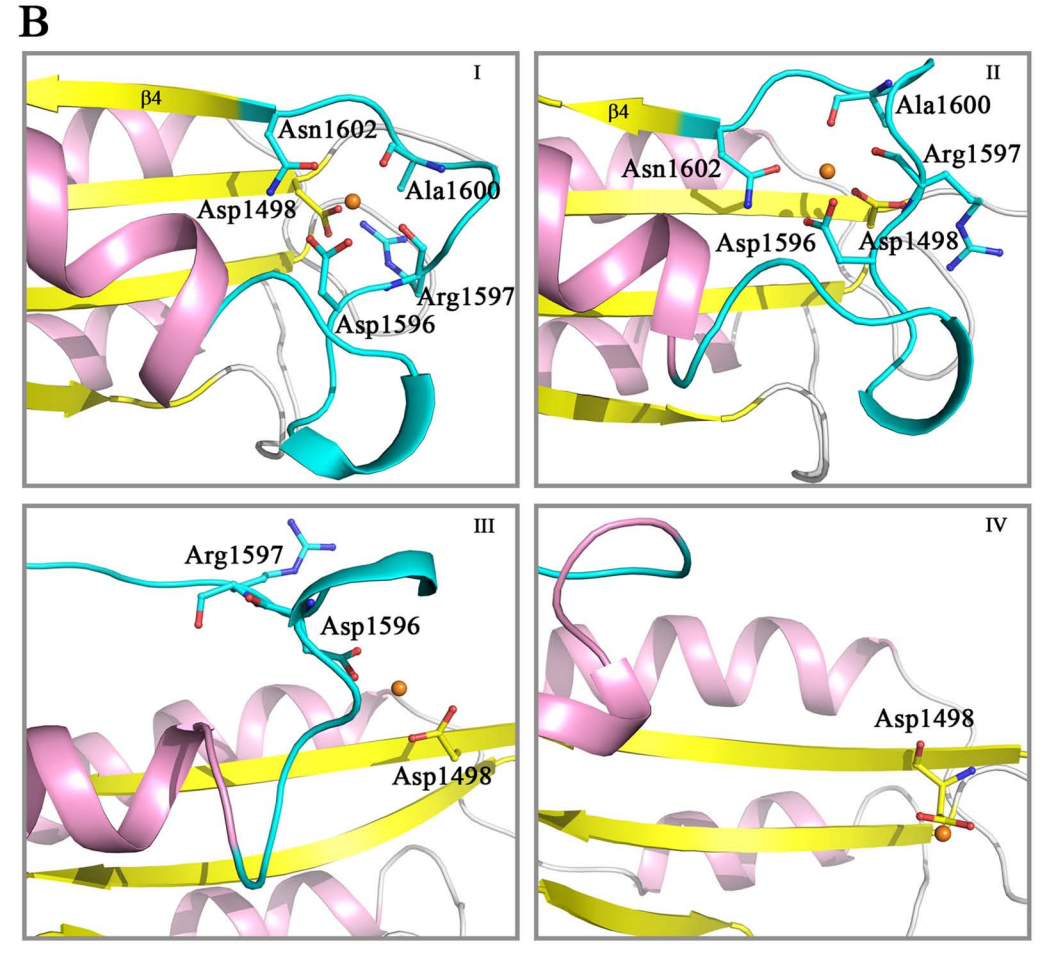
B
I
β4
Asn1602
Ala1600
Asp1498
Arg1597
Asp1596
II
β4
Ala1600
Arg1597
Asn1602
Asp1596
Asp1498
III
Arg1597
Asp1596
Asp1498
IV
Asp1498

Figure 3

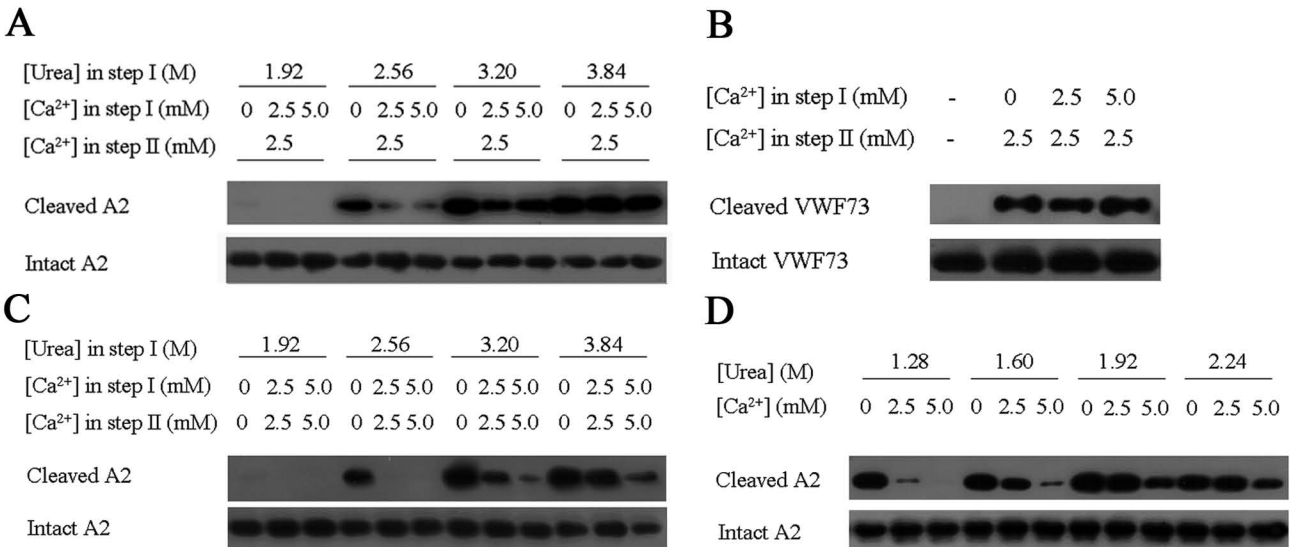
A
[Urea] in step I (M)
1.92
2.56
3.20
3.84
[Ca2+] in step I (mM)
0 2.5 5.0 0 2.5 5.0 0 2.5 5.0 0 2.5 5.0
[Ca2+] in step II (mM)
2.5
2.5
2.5
2.5
Cleaved A2
Intact A2
B
[Ca2+] in step I (mM)
-
0
2.5
5.0
[Ca2+] in step II (mM)
-
2.5
2.5
2.5
Cleaved VWF73
Intact VWF73
C
[Urea] in step I (M)
1.92
2.56
3.20
3.84
[Ca2+] in step I (mM)
0 2.5 5.0 0 2.5 5.0 0 2.5 5.0 0 2.5 5.0
[Ca2+] in step II (mM)
0 2.5 5.0 0 2.5 5.0 0 2.5 5.0 0 2.5 5.0
Cleaved A2
Intact A2
D
[Urea] (M)
1.28
1.60
1.92
2.24
[Ca2+] (mM)
0 2.5 5.0 0 2.5 5.0 0 2.5 5.0 0 2.5 5.0
Cleaved A2
Intact A2

Figure 4

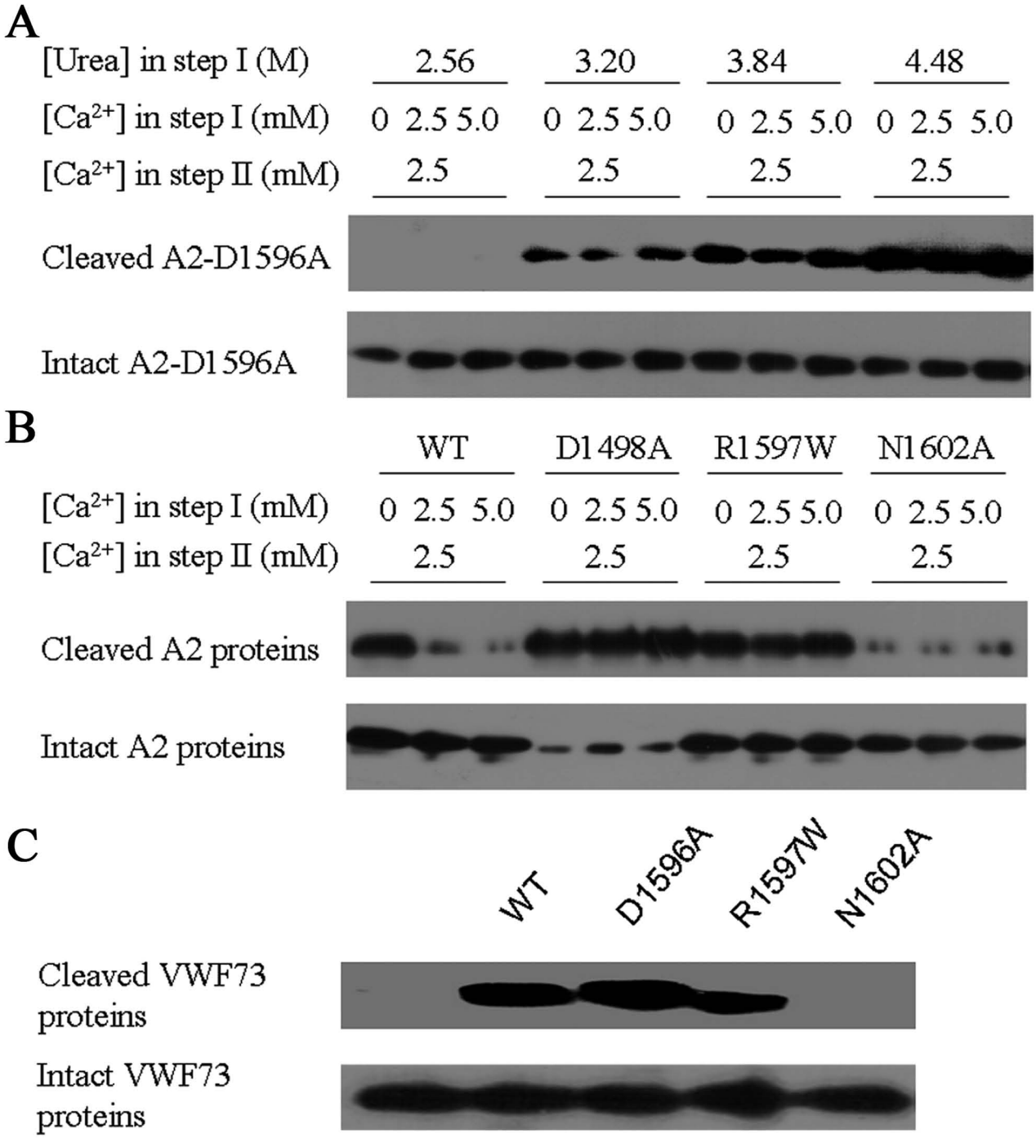
A
[Urea] in step I (M)
2.56
3.20
3.84
4.48
[Ca2+] in step I (mM)
0 2.5 5.0
0 2.5 5.0
0 2.5 5.0
0 2.5 5.0
[Ca2+] in step II (mM)
2.5
2.5
2.5
2.5
Cleaved A2-D1596A
Intact A2-D1596A
B
WT
D1498A
R1597W
N1602A
[Ca2+] in step I (mM)
0 2.5 5.0
0 2.5 5.0
0 2.5 5.0
0 2.5 5.0
[Ca2+] in step II (mM)
2.5
2.5
2.5
2.5
Cleaved A2 proteins
Intact A2 proteins
C
WT
D1596A
R1597W
N1602A
Cleaved VWF73 proteins
Intact VWF73 proteins